CONF-830910--7

CONF-830910--7

DE84 003286

FOCUSING OPTICS FOR A SYNCHROTRON X RADIATION MICROPROBE*

G. E. Ice and C. J. Sparks, Jr.

Metals and Ceramics Division, Oak Ridge National Laboratory

Oak Ridge, Tennessee 37830 USA

Submitted for Publication in

Nuclear Instruments and Methods

Third National Conference on

Synchrotron Radiation Instrumentation

September 12–14, 1983

Brookhaven National Laboratory

Upton, New York

*Research sponsored by the Division of Materials Sciences, U.S. Department of Energy under contract W-7405-eng-26 with the Union Carbide Corporation.

FOCUSING OPTICS FOR A SYNCHROTRON X RADIATION MICROPROBE*

G. E. ICE AND C. J. SPARKS, JR.
Metals and Ceramics Division, Oak Ridge National Laboratory,
Oak Ridge, TN 37830 U.S.A.

ABSTRACT

We propose two constant deviation and energy-tunable fluorescent microprobe optical designs which efficiently use x rays available from bending magnets and insertion devices of synchrotron radiation sources. The simpler system consists of a cylindrically bent multilayer to focus the vertical opening angle by in-plane scattering, a fixed radius cylindrically curved multilayer which sagittally focuses the horizontal divergence, and a pinhole to further reduce the beam to microprobe dimensions. A more versatile system has a pair of flat nondispersively arranged diffracting optics followed by crossed elliptical mirrors. These nondispersive combinations can produce a fixed-exit beam. We compare the relative intensity with other optical systems.

1. Introduction

An x-ray microprobe can be used for microdiffraction and to map the spatial distribution of elemental composition by exciting fluorescence, photo or Auger electrons. X-ray excitation has been shown [1] to have higher fluorescent yields and much larger signal-to-background ratios than charged particle excitation. This results in approximately 10^{-4} less energy deposited in the sample for the same elemental detectability and orders of magnitude lower minimum detectable limits when incident photon intensities $>10^{8}$ photons $\mu m^{-2} s^{-1}$ are achieved [1]. Because of the smaller beam spreading of x rays in the sample, the advantages of an x-ray-induced fluorescence and electron

---

*Research sponsored by the Division of Materials Sciences, U.S. Department of Energy, under contract W-7405-eng-26 with the Union Carbide Corporation.

spectroscopy could be obtained in a 1 μm-diam microprobe which competes with the spatial resolution obtained with focused electron sources in thick samples.

Best signal-to-noise requires a tunable x-ray source with as large an energy bandwidth as is compatible with the experiment. With incident radiation from 4 to 18 keV, the K or an L edge of the elements can be excited, but energies to 40 keV are desirable to excite the K shell of elements up to atomic number Z = 57. This avoids the need to detect soft L radiation from elements $41<Z<57$. X-ray energies just above the absorption edge have the highest cross section for photoionization, but bandwidths containing energy spreads as great as $\Delta E/E = 1$ can still be 37% as effective as energies just above the edge in producing ionization [1]. Thus for fluorescence and Auger spectroscopies, where the energy width of the detected radiation is independent of the energy of the exciting radiation, wide-bandpass optics are desirable. More perfect crystals will provide the narrow energy bandwidths for photoelectron spectroscopy where the energy width of the photoelectron depends on the convolution of the energy widths of the natural line, x-ray source, and detector resolution.

In this paper, mirrors, multilayer and crystal combinations are examined from the standpoint of producing the most intense image of the source, tunability, energy range and resolution, collimation, and practicality. Detailed computer-ray tracing is done to test the focusing properties of promising systems.

2. Sagittal and In-Plane Focusing

Focusing out of the plane of scatter is called sagittal focusing, and in the plane of scatter is referred to as in-plane focusing, fig. 1. For specular reflection from mirrors, ellipsoidal surfaces of revolution produce the smallest aberrations of the image. An ellipsoid combines sagittal and in-plane focusing in one doubly curved optical element. Doubly curved surfaces are used for a fixed angle of reflection as it is usually impractical to bend their radii dynamically. Mirror surfaces are also useful as substrates for the deposition of multilayers [2,3]. For microprobe applications we consider only x-ray optical designs that include multilayers or crystals to select the energy bandpass. The ideal geometry for point-to-point focusing by diffraction from multilayers consists of a confocal ellipsoid along which the multilayer "2d" spacing is varied to diffract the same energy for all rays. For Bragg diffraction from crystals where surfaces can be asymmetrically cut with respect to the diffracting planes, the ideal geometry for a point-to-point focusing x-ray monochromator is one in which the reflecting crystal planes are curved to confocal ellipsoids of revolution and the surface ground to the Rowland circle [4]. Berreman et al. [4] produced a doubly curved surface by bending the crystal, then grinding it flat before bending in the other direction. The crystallographic planes were doubly curved, but the external shape of the crystal remains cylindrical. This geometry, however, has aberrations which are too large for microprobe application where demagnifications of 10:1 or less and micron-spot sizes are required.

Elliptical, spherical, and cylindrical shapes have been proposed [1,5] that separate the in-plane and sagittal focusing to permit the use of simpler

optical surfaces. We consider the aberrations of these surfaces at small magnification. Relationships among the variables shown in fig. 1 for cylindrical surfaces are given below. For both specular reflection and symmetric diffraction,

$$N = 2F_1F_2 \sin\theta/(F_1 + F_2) , \quad (1)$$

$$R_m = N/\sin^2\theta , \quad (2)$$

and for the magnification,

$$M = F_1/F_2 . \quad (3)$$

Equation (2) is derived for the best focus in the cylindrical approximation to an elliptical surface (see fig. 2) and is not ideal for the best energy resolution. Since N increases with θ, eq. (1), the divergence accepted by the sagittal geometry is largest for crystals, then multilayers, and smallest for mirrors. A similar ranking holds for in-plane focusing. The maximum useful demagnification for sagittal focusing is limited by the ability to manufacture the necessary small radius, N. At 40 keV, sagittal demagnification is limited by the 1-cm radius to about one for specular reflection and to 6.5:1 for 40 Å (4 nm) "2d" multilayers. Demagnification is virtually unlimited for in-plane focusing. Limits to the opening angle of radiation accepted for Bragg scattering for in-plane focusing are set by the variation in $\Delta\theta = \theta_1 - \theta_2$, fig. 2. For specular reflection the critical angle, θ_c, and the magnification set a limit to the opening angle of approximately $\theta_c M/2$ for in-plane focusing without excessive comatic blurring. Even less radiation can be usefully focused because of aberrations which result when non-ideal cylindrical surfaces are used.

3. Optical Performances

We compare a spherical or cylindrical reflector in the in-plane focusing geometry and a cylindrical surface in the sagittal focusing geometry with what can be achieved with an ideal ellipsoidal and crossed elliptical surfaces. These latter two surfaces are more difficult to achieve but produce intensities near the ideal limits imposed by the opening angle of radiation which can be intercepted by a focusing reflector. Of the various possible combinations of in-plane and sagittal focusing which provide monochromatization, some of the more promising are shown in fig. 3.

fig. 3

Crossed in-plane focusing, fig. 3,B, is known as the Kirkpatrick-Baez [6] geometry. Two crossed sagittal focusing optics can be formed, but like the preceeding, the x-ray focus is moved when energy is scanned. A combination of multilayer-coated in-plane and sagittal focusing, fig. 3,D, offers fixed deviation as the reflection angle (energy) is varied, but the rays from the first optic converge onto the second at angles of incidence that deviate as a function of the magnification.

fig. 4

As shown in fig. 4, a divergent ray intercepts the two surfaces at angles that differ by $\gamma/2M$. If the rocking curve width, $\Delta\theta_B$, for the second diffracting element is compariable to $\gamma/2M$ then good transmission results. This places an upper limit to the angular acceptance, 2γ, of the optic given by

$$2\gamma(\text{max angular mismatch}) = 2\Delta\theta_B M \ . \qquad (4)$$

The first of a pair of crystal optics having small $\Delta\theta_B$ and arranged in a non-dispersive geometry must be nearly flat with no focusing [7,8]. Multilayers with large $\Delta\theta_B$ can accept angular errors from demagnifications of even 10:1.

For example, at 15 keV and an opening angle of 0.2 mrad, a 40 Å (4 nm) "2d" multilayer need have a reasonable $\Delta\theta_B/\theta_B$ of only 0.02 to diffract about 50% of the radiation from the first multilayer of the same $\Delta\theta_B/\theta_B$ and focusing at a demagnification of 10:1.

Howell and Hastings [5] have considered the case of in-plane reflection from spherical or cylindrical surfaces in the limit of small magnification. They show that spherical aberrations cause a point source to be imaged into a blur in the scattering plane, with dimensions determined by the opening angle, 2γ, of the intercepted radiation. In terms of the dimensions defined in fig. 1,B, the blur size is given by,

$$Y_m \cong 3F_1(1 + M)\gamma^2/(4M\theta) \ . \tag{5}$$

For sagittal focusing with a cylinder, a point source is blurred both in the plane of scatter and in the focal plane, fig. 1,A. For small θ, ϕ, and M, dimensions X_s and Y_s are approximately

$$X_s \cong F_1\phi^3(1 + M)^2/(4M^2\theta^2) \tag{6}$$

and

$$Y_s \cong F_1\phi^2(1 + M)/(2\theta) \ . \tag{7}$$

Equations (6) and (7) give adequate results for the aberrations for a point source when compared to exact ray-tracing methods, table 1. Typical values of the blur diameter exceed 1 μm when angular acceptances, 2ϕ, approach 0.4 mrad. This blurring of the focus limits the useful angular acceptance of the optic. Aberrations increase with larger demagnifications and smaller angles of incidence, θ.

For most cases of sagittal focusing the blur in the scattering plane, Y_s, will be more important than the blur X_s (see table 1). The image size increases when the aberration dimensions become similar to the desired probe size. With eqs. (7) and (5) we determine the opening angles of radiation which can be efficiently focused by sagittal and in-plane optical elements to be

$$2\psi_{max} \cong \theta M \sqrt{18\sigma_y/[M\theta F_1(1 + M)]} \tag{8}$$

$$2\gamma_{max} \cong \theta M \sqrt{12\sigma_y/[\theta F_1(1 + M)]} \, . \tag{9}$$

From the ratio of eq. (8) to eq. (9), we find the aberration-limited acceptance angle, 2ψ, for sagittal focusing is about four times that for in-plane focusing, 2γ. Thus, sagittal focusing is more suited for intercepting the larger angular spreads in the plane of the storage ring. When the angle of acceptance for the optic is greater than the opening angle of the source, intensity can be increased by going to smaller magnifications. Equations (8) and (9) show $2\psi_{max} \propto \theta M^{1/2}$ and $2\gamma_{max} \propto \theta M$. Thus, the angular acceptance of in-plane focusing optics decreases more rapidly with demagnification than for sagittal optics. However, in-plane focusing optics permit larger demagnifications at higher x-ray energies. For sagittal focusing with a cylinder, intensity continues to increase until aberrations in the focus smear the intensity by more than is gained by demagnification. This occurs when $X_s \cong Y_s$, leading to the minimum magnification for maximum intensity from a sagittally focusing cylinder to be expressed as

$$M_{max.int.} \cong [\sigma_y/(\theta F_1)]^{1/3} \, . \tag{10}$$

fig. 5 With the above equations and ray-tracing results, we compare in fig. 5 the intensity performance of the optical combinations shown in fig. 3. Curves in fig. 5 are identified by the same letters used in fig. 3. Practical limits placed on the size of the optics are given in the upper right-hand corner, fig. 5. We used typical design parameters for the NSLS x-ray storage ring. The one-sigma value of the vertical dimension of the source, σ_y, is 10^2 μm and in the horizontal 250 μm. At 15 keV, a 40 Å (4 nm) "2d" spacing multilayer has a Bragg angle of 0.02 rad and an assumed $\Delta E/E = 0.02$. Typical dimensions of F_1 range from 5 to 20 m. We choose the smaller value, $F_1 = 5$ m, because the angular acceptance is larger for the same aberrations and figure accuracy is less demanding.

Listed below are the various attributes of the optical combinations presented in fig. 3 with their intensity performance compared in fig. 5.

A. Nondispersive multilayers or crystals followed by an ellipsoidal mirror designed for the highest energy of operation have fixed deviation. Energy resolution could be selected by changing crystals to do microprobe analyses by fluorescence, Auger and photoelectron spectroscopies and diffraction. Practical demagnification is limited to less than 10:1 if radii smaller than 1 cm are to be avoided. Pinholes are necessary to achieve a micrometer-sized beam probe but offer the flexibility of trading flux for spatial resolution. The highest intensity at fixed energy is achieved by depositing a multilayer on an ellipsoidal surface. Energy resolution can be preserved by varying the "2d" spacing as stated previously. Larger scattering angles for multilayers reduces the accuracy required in an ellipsoidal surface figure for specular reflection [5].

B. Crossed spherical, cylindrical, or elliptical mirrors with multilayer on first element operates at a larger demagnification than A. When energy is scanned, the second optic, sample and detection apparatus pivot about the multilayer, M_1, [5]. After a demagnification of 10:1, the intensity gained on further demagnification is minimal unless elliptical mirrors are used. Demagnifications of 100:1 could possibly avoid the use of a pinhole if the necessary precision in the optical figures is met. Howells and Hastings have selected this geometry with spherical or cylindrical optics as the most cost effective for an initial effort at building a microprobe [5]. Crossed optical elements have been widely used for fixed-energy focusing systems [9].

C. Nondispersive multilayers or crystals followed by crossed elliptical mirrors have higher performance, as shown in fig. 5, than either A or B at demagnifications greater than 10:1 and at the same energy bandpass. Such an optical scheme, though somewhat more complex, has the advantages of giving fixed deviation, providing energy resolution selection by changing the diffracting elements, and achieving demagnifications of 100:1 or greater even to energies of 40 keV. Elliptical mirrors of the required figure and surface tolerance may not be too difficult to make [10]. If dynamic bending of the elliptical shape could be achieved, then demagnification could be selected to optimize the desired probe size. A consequence is that the focus moves. This is the most versatile high performance system among the various optical schemes considered, but implementation is the most difficult.

D. Nondispersive multilayers on in-plane followed by sagittal focusing optics has comparable intensity performance to that of system C but at less demagnification, thus requiring a pinhole to collimate to a spatial resolution approaching 1 μm. It is not suitable for use with nearly perfect crystals as discussed earlier. Simple cylindrical surfaces are used and fixed deviation is possible. In table 2 we compare at 15 keV the ray-tracing results from a nondispersive multilayer system (fig. 3,D), a Kirkpatrick-Baez system (fig. 3,B), and an ideally doubly curved germanium (111) crystal. In the multilayer system, the variation in "2d" from deposition onto a surface of varying slope was included.

table 2

We discuss in the following section the possible implementation of D as it is both a practical and high performance system for an initial microprobe with multilayers in an energy-tunable fixed-deviation focusing system.

4. Design Considerations

A practical optical design for a fluorescence and Auger microprobe is one which combines two multilayers, one to in-plane focus the vertical divergence, and one to sagittally focus the horizontal divergence as shown in fig. 2,D. A pinhole as the last optical element minimizes the sensitivity of the optics to aberrations and takes advantage of the maximum intensity obtained at relatively modest demagnifications.

To scan energy, the radius of the first multilayer must change. Since the radius is large (several meters) for in-plane focusing and small (few centimeters) for sagittal focusing, transverse or anticlastic bending is insignificant for in-plane focusing but must be controlled in sagittal focusing [8]. This makes in-plane focusing easier since the multilayers or

crystals do not have to be reinforced against transverse bending. Reinforcing ribs would spoil the image unless rib thicknesses half the focus diameter could be achieved or other methods found [8]. To avoid transverse bending, we propose to polish the sagittally focusing cylinder to a fixed radius. To maintain a fixed radius for the sagittal cylinder and a fixed focus, the two-multilayer system can be translated along the beam direction as energy is changed so that the sagittal radius always satisfies eq. (1). Translations less than 0.5 m will permit a scan over an energy range from 4 to 18 keV with a fixed radius. Higher energies require exchanging the sagittal cylinder for one of smaller radius. The angular acceptance is very nearly constant over the entire energy range. It is proposed that the two optics have a fixed separation (like a channel cut crystal), and the diffracted beam from the first optic scans along the sagittal optic as energy is changed. This vertical displacement and that from bending the in-plane optic can be held constant by adjustments in the bending device.

Multilayers with scattering angles only four times greater than those from mirrors will specularly reflect x rays of about one-fourth the energy of those diffracted. To optimize the performance of a fluorescent microprobe, the low energy radiation specularly reflected by the multilayers should be minimized. This radiation is scattered by the sample into the detector and contributes to background beneath the fluorescent peaks of interest. Scattering can be reduced by proper orientation of the detector with respect to the incident beam direction and polarization vector. Low Z filters can be used to attenuate specular reflection with only a modest decrease in transmission of the multilayer's diffracted energy. The absorption cross section of the low Z

filter is approximately proportional to E^{-3}. A calculated spectrum assuming a constant intensity versus energy impinging on the multilayer is shown in fig. 6, where TO = 1 is the diffracted and specularly reflected intensity off the multilayer when no filter is used. If we use a filter which transmits 50% (TO = 0.5 in fig. 6) of the diffracted energy from the multilayer, then the specular reflected intensity off the multilayer is less than 10^{-5} of the diffracted intensity.

The first multilayer could be deposited on a bendable flat substrate. The second multilayer is to be deposited on a substrate that is cylindrically curved. Because multilayer deposition is not normal to the sloping sides of the substrate, the "2d" spacing varies according to the relation "2d" = $2d_0 \cos\phi$ where d_0 is the central ray and $\phi = F_1\phi/N$. From eqs. (1) and (8), it can be shown that the maximum change in "2d" is about 0.6%. This small variation at the extremes of the acceptance degrades transmission by about 3% when multilayers with $\Delta E/E = 0.02$, FWHM are used. All calculations comparing intensity performance included this variation in "2d" spacing.

The final optical element is a precision pinhole. An 80 μm-thick gold foil will transmit one part in 10^7 of the incident radiation at an energy up to 18 keV. To prevent the beam from diverging excessively both the distance from the pinhole to the sample and the beam penetration into the sample must either be limited or the beam divergence restricted. Typical beam penetration depths for 95% of the maximum fluorescent yield are given in fig. 7. We use a pessimistic assumption that the fluorescent energy coming out of the sample is the same as the incident energy which is identified as 10, 20, and 40 keV on the curves. The sketch in the upper right of fig. 7 relates the divergence

angle, δ, and the beam spreading, D, to the distance, L, away from the pinhole. Since $D/\delta = L$, the right-hand ordinate gives the values of the ratio D/δ which correspond to the values of L in micrometers on the left-hand ordinate. To preserve the resolution of a 1-μm-diam pinhole, we limit the beam spread, D, to about 1 μm. If δ = 1 mrad, then $D/\delta = 1\ \mu m \cdot mrad^{-1}$, and (reading directly across the figure) the left-hand ordinate gives 10^3 μm for L. Thus, the total distance L of 10^3 μm which preserves D at 1 μm is the sum of the distance from the pinhole to the sample surface plus the penetration of the beam into the sample for 95% fluorescent yield. At 10^3 μm, most samples with elements averaging above 20 in atomic number and at x-ray energies below 20 keV would preserve the probe resolution if we limit the distance between the pinhole and the sample to a few hundred micrometers. Diffraction blurring from the pinhole aperture is negligible compared to a 1 μm image size.

5. Conclusion

We have defined two energy-tunable and fixed-deviation systems: one is very versatile with crossed elliptical mirrors for in-plane focusing; the other a simpler design of in-plane and sagittal optics. Since less than one milliradian is required to achieve maximum intensity from even the most favorable optics, a microprobe is most effectively served by undulator devices on storage rings with small source sizes. A reduction in the source area by a factor of ten improves the intensity by a factor of five. Estimated fluxes for the nondispersive focusing multilayer geometry using several possible NSLS sources are listed in table 3. We note that photon intensities orders of magnitude above 10^8 photons $s^{-1}\ \mu m^{-2}$ are possible. Even higher intensities are possible using undulators in multi-GeV storage rings. Undulators and

table 3

wiggler magnets produce about the same number of photons cm^{-1} of length, but undulators confine the radiation to smaller opening angles and a more narrow energy spectrum. Anticipated intensities with a feasible undulator in PEP at 15 GeV and 15 mA are estimated to be 10^{14} photons s^{-1} μm^{-2} at 10 keV. Intensity could then be sacrificed to achieve spatial resolutions approaching 500 Å (50 nm) at 15 keV determined by the diffraction limit from a pinhole aperture and a specimen-to-pinhole distance of 100 μm.

REFERENCES

[1] C. J. Sparks, Jr., *Synchrotron Radiation Research,* eds. H. Winick and S. Doniach (Plenum, New York, 1980) Chap. 14.

[2] T. W. Barbee, Jr., *AIP Conference Proceedings No. 75 on Low energy x-ray diagnostics* (1981) 131.

[3] D. H. Bilderback, B. M. Lairson, T. W. Barbee, Jr., G. E. Ice, and C. J. Sparks, Jr., *Nucl. Instr. & Meth.* 208 (1983) 251.

[4] D. W. Berreman, J. Stamatoff, and S. J. Kennedy, *Appl. Opt.* 16 (1977) 2081.

[5] M. R. Howells and J. B. Hastings, *Nucl. Instr. & Meth.* 208 (1983) 379.

[6] P. Kirkpatrick and A. V. Baez, *J. Opt. Soc. Am.* 38 (1948) 766.

[7] C. J. Sparks, Jr., B. S. Borie, and J. B. Hastings, *Nucl. Instr. & Meth.* 172 (1980) 237.

[8] C. J. Sparks, Jr., G. E. Ice, J. Wong, and B. W. Batterman, *Nucl. Instr. & Meth.* 194 (1982) 73.

[9] N. G. Webb, S. Samson, R. M. Stroud, R. C. Gamble, and J. D. Baldeschwieler, *J. Appl. Cryst.* 10 (1977) 104; J. C. Haselgrove, A. R. Farugi, H. E. Huxley, and U. W. Arndt, *J. Phys. E.* 10 (1977) 1035; J. Hendrix, M.H.J. Koch, and J. Bordas, *J. Appl. Cryst.* 12 (1979) 467.

[10] J. H. Underwood and D. Turner, in *Proceedings of SPIE* 106 (1977) 125.

Table 1

Ray tracing results verify the usefulness of equations (6) and (7) for predicting the aberrations from cylindrical surfaces in sagittal focusing geometry.

Design Parameters	ψ 0.5 Divergence Angle (mrad)	X_S Ray Tracing (μm)	X_S Eq. (6) (μm)	Y_S Ray Tracing (μm)	Y_S Eq. (7) (μm)
M = 1/5	0.1	0.1	0.1	1.4	1.5
Fl = 5 m	0.2	1.0	0.9	5.8	5.8
sinθ = 0.02					
M = 1/20	0.1	1.3	1.3	1.2	1.3
F^1 = 5 m	0.2	11.0	11.0	4.4	5.1
sinθ = 0.02					
M = 1/10	0.1	0.024	0.038	0.45	0.44
F^1 = 5 m	0.2	0.3	0.3	1.7	1.8
sinθ = 0.06					

Table 2

Comparison of various focusing optics at 15 keV.

	Divergence on sample (mrad)	Image size (μm^2)	Transmission[a]	Intensity[b]
Nondispersive multilayers, M = 1/10, with pinhole	2.4 × 0.3	24.0 × 16	56.00	0.2
Kirkpatrick-Baez multilayer at M = 1/100, mirror at M = 1/200	0.3 × 0.3	2.4 × 1	0.04	0.02
Doubly curved Ge (111), symmetrically cut, M = 1/10	2.8 × 0.6	31.0 × 15	5.00	0.01

[a] Transmission before final pinhole in ev · mrad.

[b] Relative intensity in 1 μm^2 spot on the sample in ev · mrad · μm^{-2}.

Table 3

Expected intensities from NSLS sources (500 mA at 2.5 GeV) with nondispersive multilayers in in-plane followed by sagittal focusing (photons μm^{-2}).

NSLS sources	5 keV	15 keV
Arc	1.4×10^{12}	2.5×10^{10}
Hybrid wiggler	6.0×10^{13}	1.0×10^{12}
Superconducting wiggler	8.0×10^{12}	1.0×10^{12}

FIGURE CAPTIONS

Fig. 1 The two kinds of focusing geometry and the parameters used to calculate aberrations in their focal spots.

Fig. 2 The elliptical shape ideally reimages a point from the source, S, at the image, i, for specular reflection. Segments of the elliptical surface are approximated by a circle of radius R_m. Variation in scattering angle, θ, across the surface limits the angular acceptance of the ellipse and other shapes when in-plane focusing is used with symmetrically cut Bragg diffracting elements.

Fig. 3 X-ray optical configurations for forming high intensity images of synchrotron radiation sources. The ellipsoidal surface combines both sagittal and in-plane focusing into one optical element. Combinations of separated in-plane and sagittal focusing produce optical systems with varying capabilities.

Fig. 4 In-plane focusing requires that the Bragg acceptance angle of the following sagittal focusing optic be large enough to diffract over the convergence anglar range, $2\gamma/M$.

Fig. 5 The relative intensity for various x-ray optical configurations identified in fig. 3 is plotted against the magnification for the given parameters. One centimeter is chosen as the manufacturing limit achievable for the radius of curvature of a mirror surface.

Fig. 6 Specular reflection of lower energy x rays occurs from multilayers since Bragg diffraction angles are only a few times larger than the critical angle for total reflection. Filters which transmit various fractions of the diffracted energy (T0 = 0.5 is 50% transmission of the diffracted radiation) reduce the reflected energies by several orders of magnitude.

Fig. 7 The depth that x rays penetrate into a sample of atomic number Z to achieve 95% of the maximum fluorescent yield is calculated assuming that the fluorescent energy is the same as the exciting x-ray energy of 10, 20, or 40 keV. Convergence angles, δ, cause the beam to spread and must be limited so that the depth of x rays penetrating into the sample preserve the desired probe size, D. See text for use of this figure to determine δ.

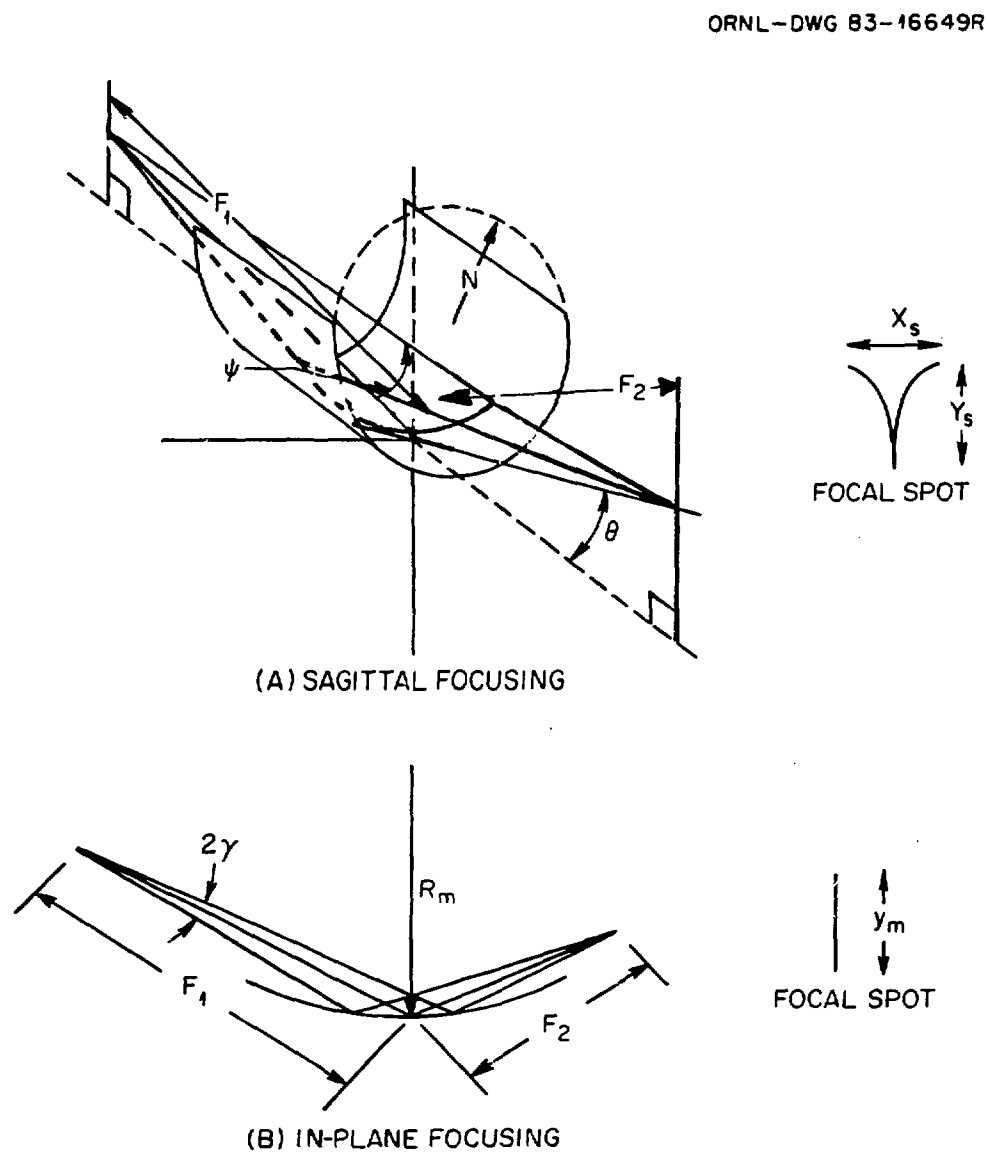

Fig. 1 The two kinds of focusing geometry and the parameters used to calculate aberrations in their focal spots.

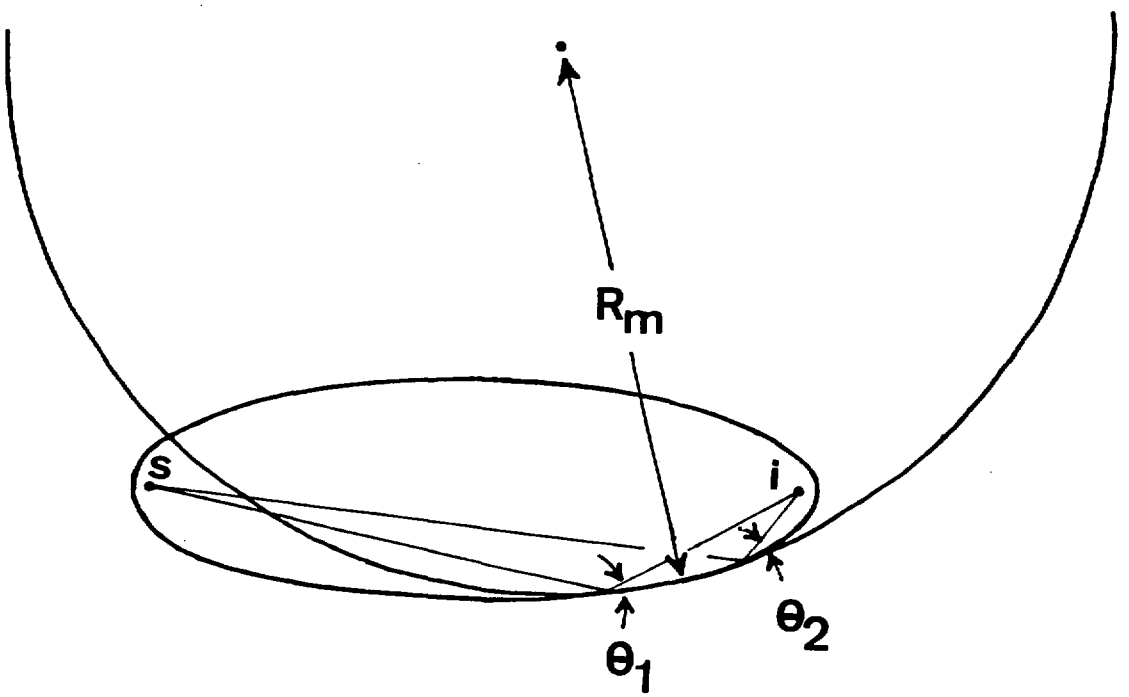

Fig. 2 The elliptical shape ideally reimages a point from the source, S, at the image, i, for specular reflection. Segments of the elliptical surface are approximated by a circle of radius R_m. Variation in scattering angle, θ, across the surface limits the angular acceptance of the ellipse and other shapes when in-plane focusing is used with symmetrically cut Bragg diffracting elements.

ORNL-DWG 83-16646R

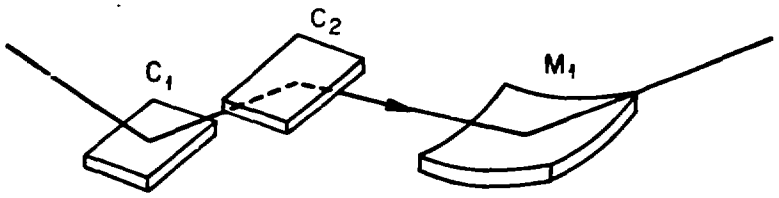

(A) NONDISPERSIVE MULTILAYERS OR CRYSTALS FOLLOWED BY ELLIPSOIDAL MIRROR

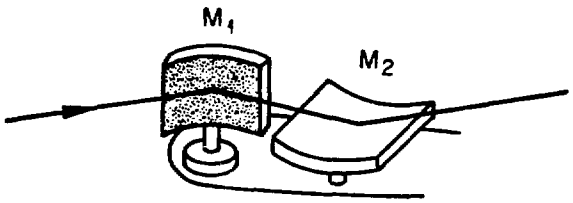

(B) CROSSED SPHERICAL OR ELLIPTICAL MIRRORS WITH MULTILAYER ON M_1

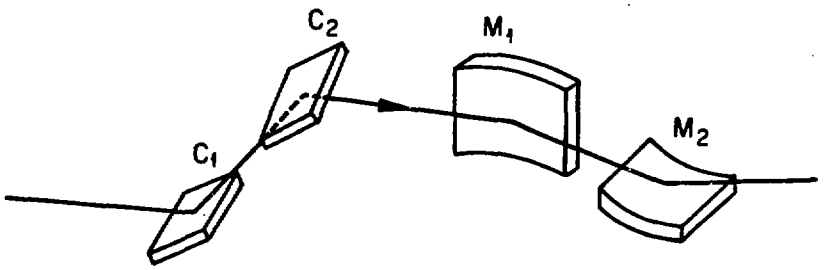

(C) NONDISPERSIVE MULTILAYERS OR CRYSTALS FOLLOWED BY CROSSED ELLIPTICAL MIRRORS

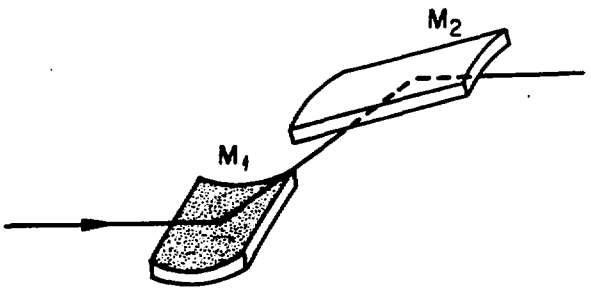

(D) NONDISPERSIVE MULTILAYERS ON BOTH MIRRORS M_1 (CYLINDRICAL OR SPHERICAL) AND M_2 (CYLINDRICAL)

Fig. 3 X-ray optical configurations for forming high intensity images of synchrotron radiation sources. The ellipsoidal surface combines both sagittal and in-plane focusing into one optical element. Combinations of separated in-plane and sagittal focusing produce optical systems with varying capabilities.

ORNL-DWG 83-17219R

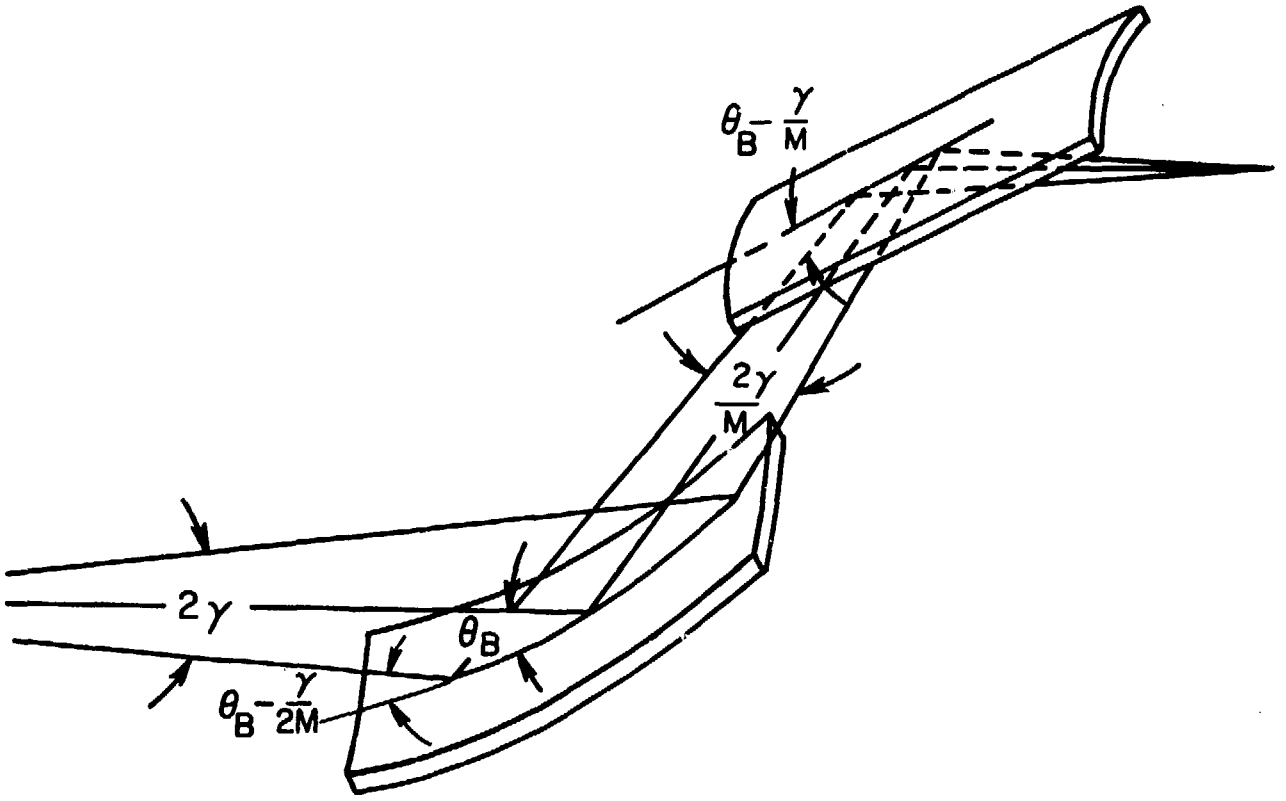

Fig. 4 In-plane focusing requires that the Bragg acceptance angle of the following sagittal focusing optic be large enough to diffract over the convergence anglar range, $2\gamma/M$.

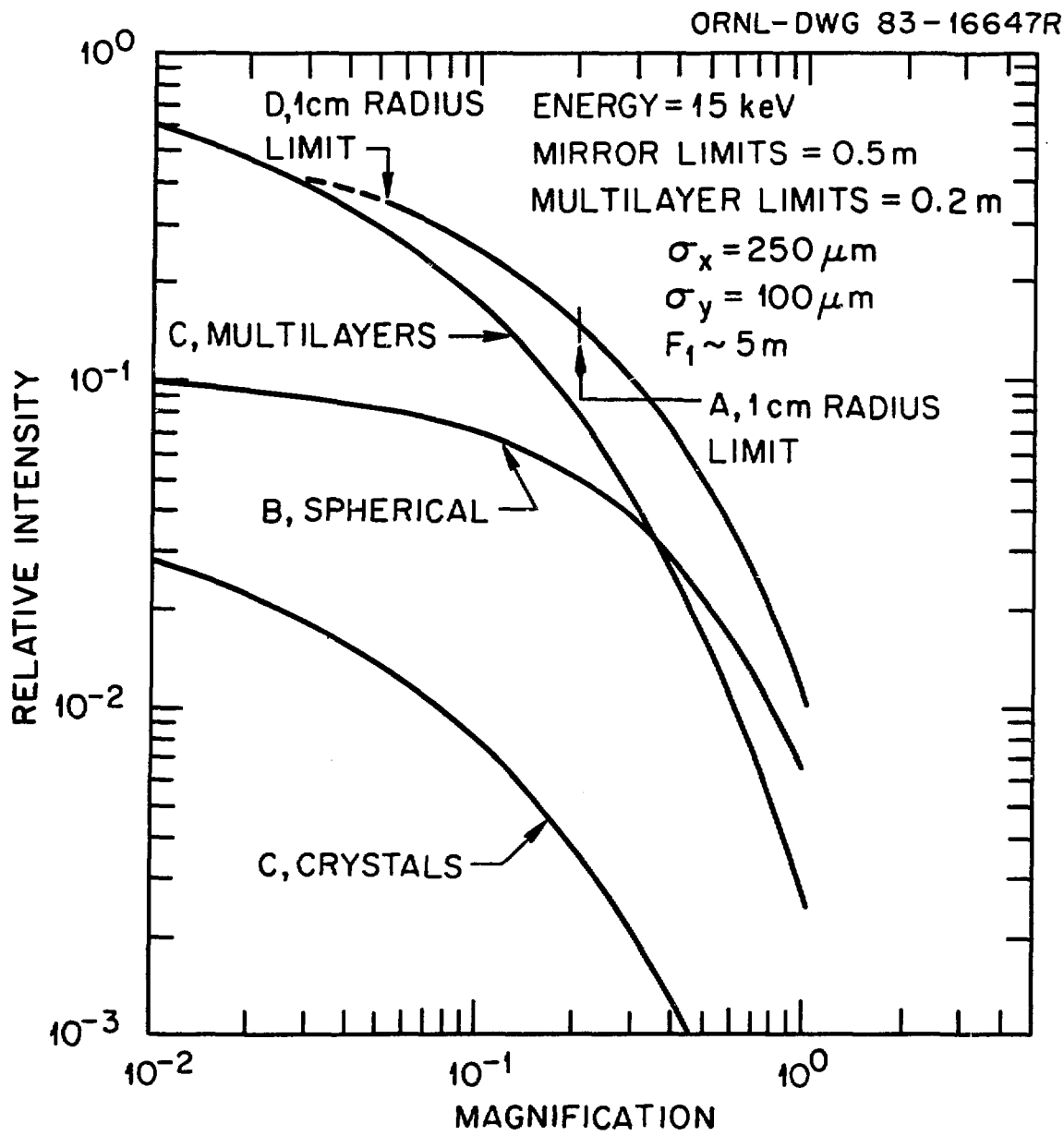

Fig. 5 The relative intensity for various x-ray optical configurations identified in fig. 3 is plotted against the magnification for the given parameters. One centimeter is chosen as the manufacturing limit achievable for the radius of curvature of a mirror surface.

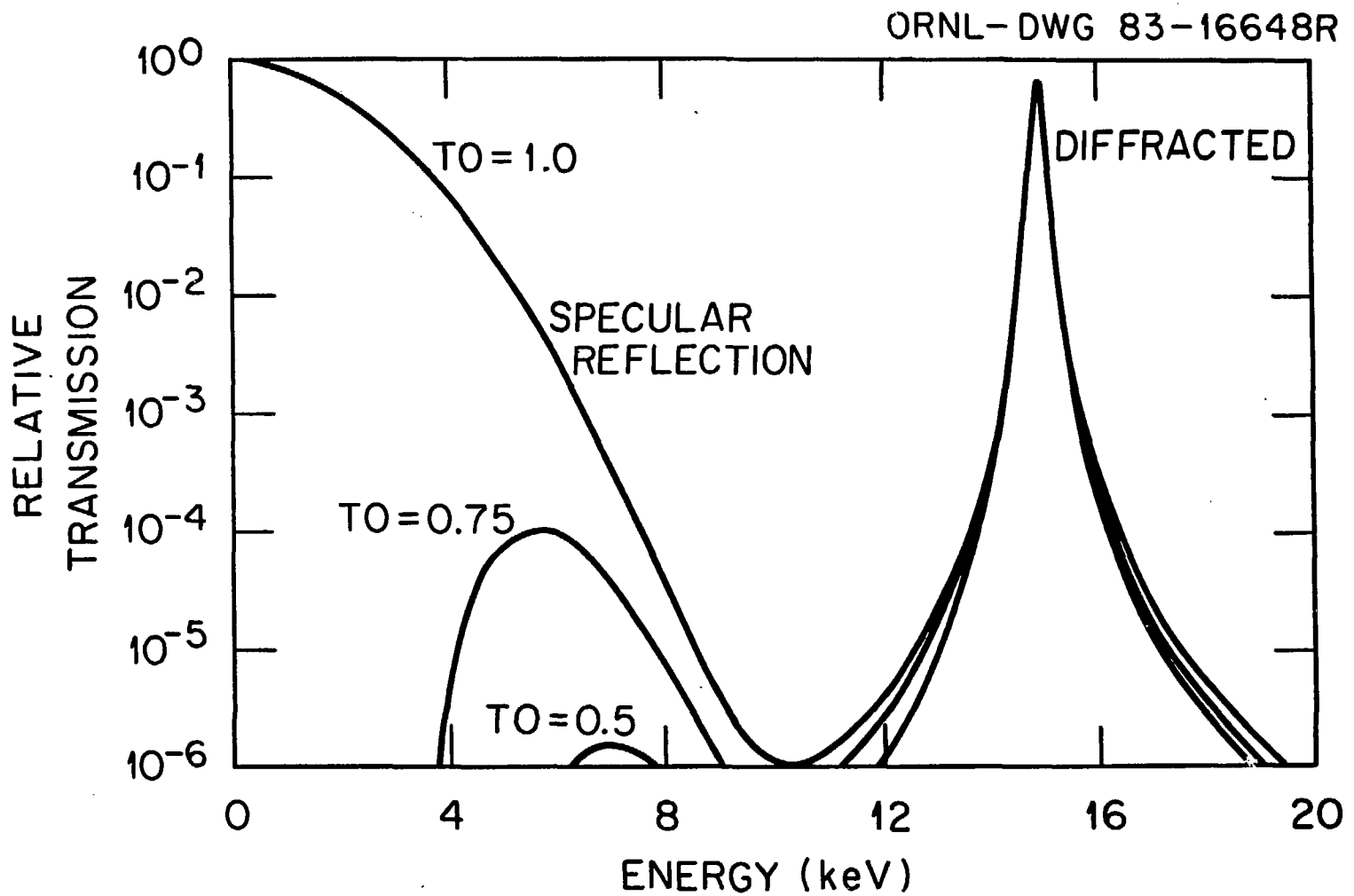

Fig. 6 Specular reflection of lower energy x rays occurs from multilayers since Bragg diffraction angles are only a few times larger than the critical angle for total reflection. Filters which transmit various fractions of the diffracted energy (TO = 0.5 is 50% transmission of the diffracted radiation) reduce the reflected energies by several orders of magnitude.

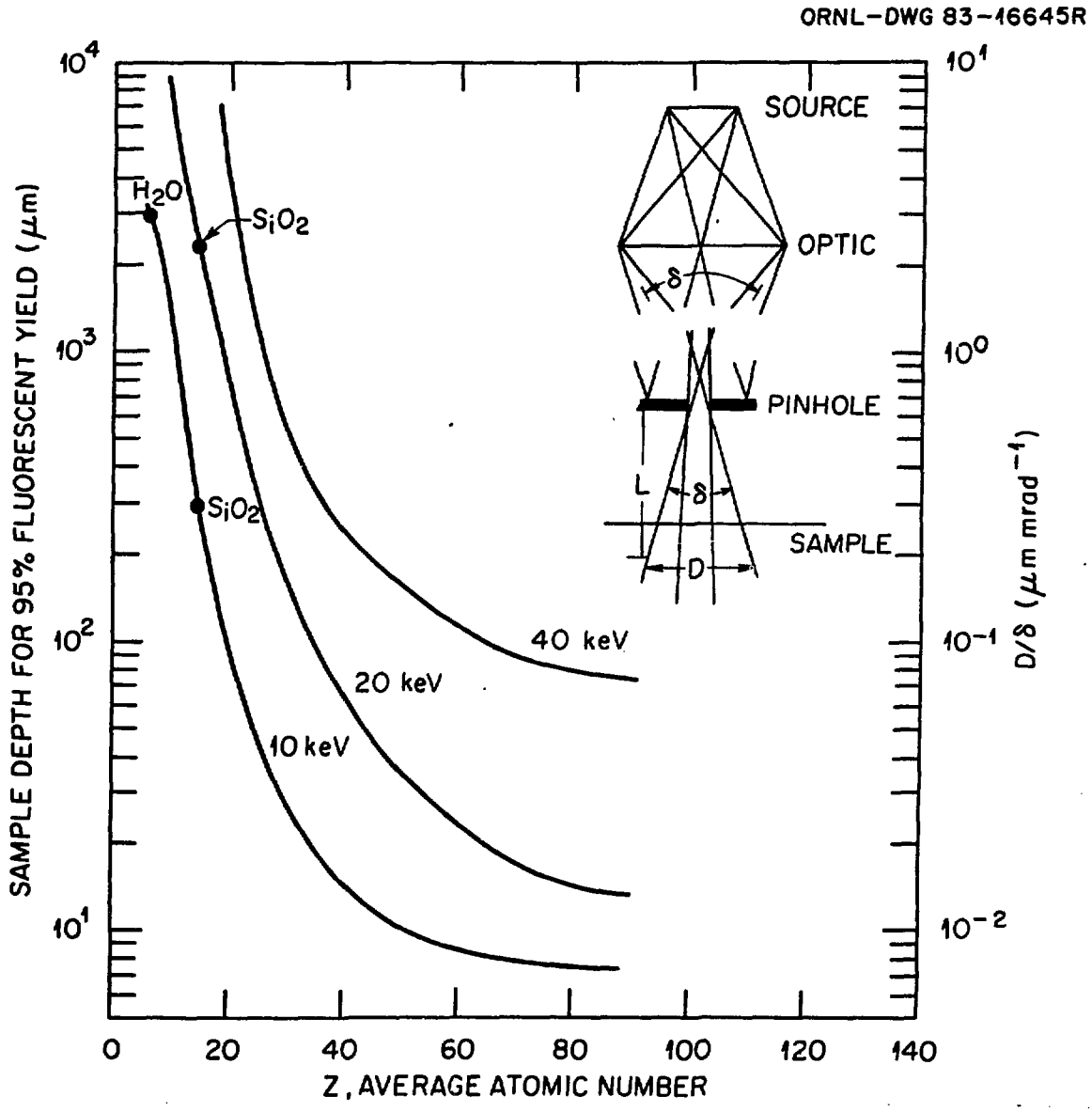

Fig. 7 The depth that x rays penetrate into a sample of atomic number Z to achieve 95% of the maximum fluorescent yield is calculated assuming that the fluorescent energy is the same as the exciting x-ray energy of 10, 20, or 40 keV. Convergence angles, δ, cause the beam to spread and must be limited so that the depth of x rays penetrating into the sample preserve the desired probe size, D. See text for use of this figure to determine δ.